Subwavelength plasmonics for graded-index optics on a chip

Meir Grajower,[1] Gilad M. Lerman,[1] Ilya Goykhman,[1] Boris Desiatov,[1] Avner Yanai,[1] David R. Smith,[2] and Uriel Levy[1,*]

[1]*Department of Applied Physics, The Benin School of Engineering and Computer Science, The Center for Nanoscience and Nanotechnology, The Hebrew University of Jerusalem, Jerusalem 91904, Israel*

[2]*Center for Metamaterials and Integrated Plasmonics, Department of Electrical and Computer Engineering, Duke University, Durham, North Carolina 27708, USA*

**Corresponding author: ulevy@cc.huji.ac.il*

Received June 3, 2013; revised July 28, 2013; accepted August 7, 2013; posted August 12, 2013 (Doc. ID 191642); published September 4, 2013

Planar plasmonic devices are becoming attractive for myriad applications, owing to their potential compatibility with standard microelectronics technology and the capability for densely integrating a large variety of plasmonic devices on a chip. Mitigating the challenges of using plasmonics in on-chip configurations requires precise control over the properties of plasmonic modes, in particular their shape and size. Here we achieve this goal by demonstrating a planar plasmonic graded-index lens focusing surface plasmons propagating along the device. The plasmonic mode is manipulated by carving subwavelength features into a dielectric layer positioned on top of a uniform metal film, allowing the local effective index of the plasmonic mode to be controlled using a single binary lithographic step. Focusing and divergence of surface plasmons is demonstrated experimentally. The demonstrated approach can be used for manipulating the propagation of surface plasmons, e.g., for beam steering, splitting, cloaking, mode matching, and beam shaping applications.

OCIS codes: (240.6680) Surface plasmons; (220.3630) Lenses.
http://dx.doi.org/10.1364/OL.38.003492

In the last decade, the field of plasmonics has grown rapidly, as evidenced by the rapid increase in journal publications and scientific activity. Following this extensive research effort, numerous applications are now arising, including microscopy [1–3], on-chip optoelectronic circuitry [4–6], enhancement of nonlinear processes [7,8], sensing [9–11], nanolithography [12], nanomemories [13,14], light sources [15,16], and nanodetectors [17–21] to name a few. A common need for many of these applications is the capability of controlling the propagation of surface plasmon polaritons (SPPs) along the metal–dielectric interface. Specifically, the capability of focusing SPPs is of great interest, leading to the demonstration of various designs of plasmonic lenses [22–24].

In parallel, the field of transformation optics and graded-index optics is gaining growing attention, with applications such as cloaking driving it forward. Several 2D realizations of transformation optics and graded-index focusing in the visible/near-IR domain were demonstrated in recent years [25–29]. For example, graded-index optics and cloaking were demonstrated in a silicon photonics platform by carving subwavelength features in a silicon slab, taking advantage of the concept of effective index to engineer the local effective refractive index of the silicon slab at will. In this Letter, we take advantage of this effective refractive index concept in order to demonstrate a graded-index plasmonic lens that can focus SPPs in a plane comprising a metal–dielectric interface. This approach is complimentary to that of gray-scale lithography, where the thickness of the dielectric film controls the local effective index of the plasmonic mode [24]. The demonstrated concept may serve as a powerful tool to be used, e.g., in future plasmonic-based transformation optics systems capable of manipulating the SPP mode for the desired application.

In order to focus an electromagnetic wave propagating within a medium, the refractive index profile of the medium must vary along the direction perpendicular to the propagation direction. A simple parabolic profile for the index can provide reasonable focusing qualities, though more complex profiles can be used to reduce certain geometrical aberrations [30]. The well-known gradient-index (GRIN) lens, commonly used in optics, is an example of an optical device that makes use of a spatially inhomogeneous index profile. Due to their fields being confined to the metal-dielectric interface in the direction perpendicular to the interface, SPP waves can be focused by the use of a planar graded-index profile created in-plane transverse to the direction of wave propagation.

From the above discussion, an effective refractive index profile that will produce the in-plane equivalent of a lens might have the form

$$n = n_0\left(1 - \frac{1}{2}\alpha x^2\right), \tag{1}$$

where n_0 is the on-axis effective refractive index, α is the curvature of the refractive index profile, and x is the distance from the optical axis.

The SPP mode is confined at the interface between a metal having negative permittivity and a dielectric having positive permittivity. In this work, the SPP is propagating in a slab consisting of 240 nm thick layer of polymethyl methacrylate (PMMA) on top of a thick Au film. As previously shown [31,32], at frequencies much lower than the surface plasmon resonance frequency, where most of the electromagnetic energy resides in the dielectric medium, one can manipulate the SPP propagation by controlling its effective index via modifying the thickness of the dielectric layer. Yet, the effective index can also be

precisely controlled by defining subwavelength features in the dielectric medium. Following this concept our device is based on the patterning of a subwavelength grating in the PMMA, where the duty cycle of the grating is locally modulated in order to achieve the desired parabolic effective index profile.

As an estimate for the relation between the duty cycle and the local effective refractive index of the SPP mode we use the effective medium theory (EMT) [33]. First, we calculated the effective refractive index of the SPP mode propagating within a uniform layer structure consisting of 240 nm thick PMMA (having refractive index of about 1.49 at the wavelength of 1550 nm) sandwiched between Au and air, and found it to be $n_{\mathrm{EP}} = 1.21746 + j0.0034$. The other extreme case, in which the PMMA layer is replaced by air, results in an effective refractive index of $n_{\mathrm{EA}} = 1.0038 + j0.004$. Next, we use these two values to calculate the effective refractive index as a function of the duty cycle of the PMMA grating:

$$n_{\mathrm{TE}}^{(2)} = \sqrt{n_{\mathrm{TE}}^{0} + \frac{1}{3}\left(\frac{\Lambda}{\lambda}\pi f(1-f)(n_{\mathrm{EP}}^{(2)} - n_{\mathrm{EA}}^{(2)})\right)^{2}}, \quad (2)$$

where $n_{\mathrm{TE}}^{0} + \sqrt{f n_{\mathrm{EP}}^{2} + (1-f) n_{\mathrm{EA}}^{2}}$ is the zero-order effective refractive index, λ is the wavelength, Λ is the grating period, and f is the fill factor (duty cycle). This approximation is reasonably valid as long as $\Lambda \ll \lambda/n_{\mathrm{EP}}$. It should be mentioned that because of the space-variant nature of the structure, the Bloch theorem cannot be applied in its direct form. Additionally, one should notice the notation of polarization. Here, TE corresponds to a case where the electric field is transverse to the grating period, i.e., oriented along the y axis. This is a common definition within the scientific community working on grating structures. However, with regard to the plasmonic layered structure this polarization should be coined TM. Thus, the SPP mode is supported at the metal-dielectric interface.

The lens is designed for an incident beam width of 13 μm. Additionally, we constrain the minimal and maximal PMMA linewidths to 140 and 280 nm, respectively. Setting the period to be $\Lambda = 400$ nm (well within the subwavelength limit for 1.55 μm wavelength) these values correspond to duty cycles of 0.35 and 0.7, respectively. Using these values in Eq. (2), one obtains maximal and minimal effective index of $n_{\mathrm{min}} = 1.084 + j0.0016$ and $n_{\mathrm{max}} = 1.158 + j0.0026$ respectively. As a result, the curvature of the refractive index profile is found to be $\alpha = 0.003[1/(\mu\mathrm{m})^2]$.

Having these values set, one can now calculate the local effective refractive index of the plasmonic mode [Fig. 1(b)] and a typical mode profile [Fig. 1(a)]. Figure 1(c) shows a top view of the designed PMMA grating distribution, which creates the parabolic refractive index.

Based on the calculated quadratic refractive index profile and assuming the paraxial approximation to be valid, we calculated the beam profile at each plane along the propagation direction using the ABCD matrix method and found the focal length of the lens to be 28.67 μm.

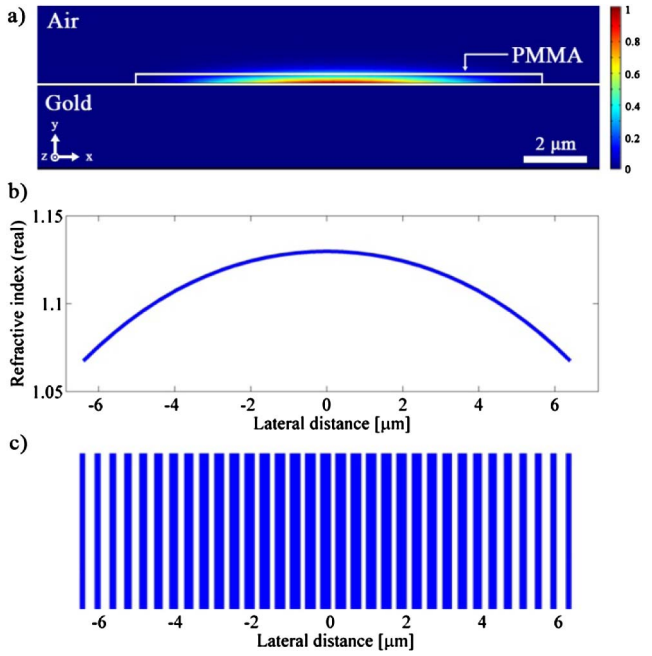

Fig. 1. (a) Longitudinal Poynting vector (P_z) of the SPP mode confined at the Au–PMMA interface. Transverse confinement is achieved owing to the graded-index distribution of the PMMA layer. (b) The effective parabolic refractive index of the SPP lens (real part) and (c) the PMMA nanobars width which creates the effective parabolic refractive index plotted in (b).

To verify the validity of the various assumptions made along the design, we simulated the propagation of light within the designed structure using a full-wave 3D finite-difference time-domain (FDTD) simulation. Figure 2 shows the magnetic field intensity (H_x) distribution. The focus is obtained at a distance of ~22 μm from the excitation source. The difference between the calculation based on the ABCD matrix method and the FDTD simulation result is reasonable and can be explained by the quantization of the refractive index of the lens, the use of effective medium approximation, and by the deviation from the paraxial approximation.

After validating our design we turned to the fabrication of the actual device. First, a thin film of Cr (5 nm) followed by a thicker layer of Au (50 nm) was evaporated on top of a silicon chip. Next, a 240 nm thick PMMA layer was spin coated on top of the metal. Finally, the

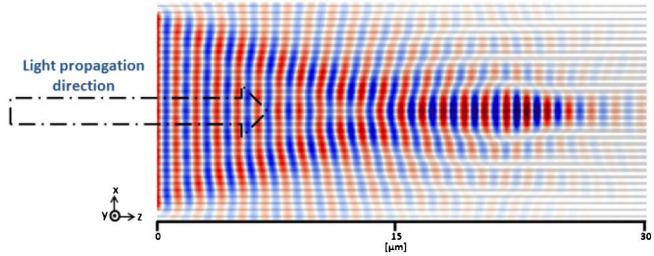

Fig. 2. 3D FDTD simulation of light propagating within the graded-index plasmonic lens structure. The simulation was performed by MEEP [34]. The major magnetic field (H_x) at the interface between PMMA and air is shown. As can be seen, the plasmonic beam is converging toward a focus located ~22 μm away from the excitation source.

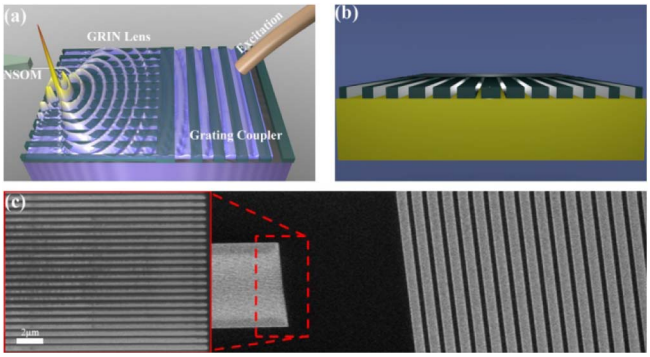

Fig. 3. (a) Schematic drawing showing an overview of the device and the experimental setup including the grating coupler and the graded-index plasmonic lens, the excitation fiber, and the NSOM tip. The scheme illustrates the focusing of the SPP mode as it propagates along the graded-index lens. (b) Cross section of the graded-index lens demonstrating the space variant duty cycle of the PMMA grating; (c) Scanning electron micrograph of the fabricated device. On the right we can observe the grating coupler and the graded-index section. The box on the left is a zoom-in on the dashed region, showing a portion of the graded-index lens.

subwavelength grating pattern was defined in the PMMA layer using E-beam lithography. In addition, a grating coupler was also patterned in the PMMA to facilitate the coupling of light from free space into the device. This coupling grating consisted of 50 periods of 80 μm long PMMA lines with a period of $\Lambda = 1.95$ μm and duty cycle of nearly 50%. Our computer simulations show that such a grating structure supports the coupling of a plane wave at an incident angle of 30° with respect to the normal direction of the sample into SPP mode. To ease on the measurement apparatus, a 5 μm long uniform PMMA section was kept between the coupler and the lens. A schematic drawing of the fabricated structure, along with scanning electron micrograph image of the grating profile can be seen in Fig 3.

To measure the propagation of the SPP wave within the structure, we coupled light derived from a diode laser source at 1550 nm wavelength into a bare single-mode fiber. The fiber was positioned at an angle of 30 deg with respect to the normal direction of the device and its position was controlled by a high-precision translation stage. The SPP wave propagation was directly measured by a near-field scanning optical microscope (NSOM, Nanonics MultiView 4000) with a probe of 300 nm diameter. A schematic sketch of the experimental setup is shown in Fig. 3(a).

The NSOM measurement results are shown in Fig. 4. Figure 4(a) shows the intensity distribution with brighter color corresponding to higher intensity. As can be seen, the wavefront is converging toward the beam waist, which is located 23.5 μm away from the front end of the lens. This is clearly shown by the zoom-in section on the right. After obtaining its minimum size, the beam diverges as it further propagates beyond the focal point. Figure 4(b) shows the measured intensity across the focus (transverse direction).

Interestingly, even though our NSOM measures the intensity of light rather than field (we did not use a heterodyne interferometric approach), the wavefronts

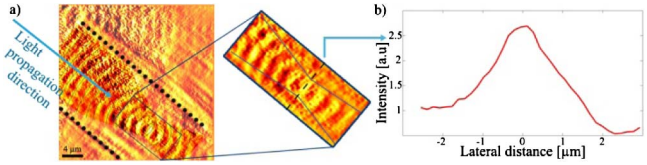

Fig. 4. NSOM measurement: (a) NSOM signal measuring the light propagation down the lens (between the two black lines) with wavefront as been calculated, in the box—zoom-in on the focus point and (b) a transverse cross section of (a) in the focal plane, which is marked by the dashed line in the zoom-in section.

can be clearly observed. We attribute this to the interference between the SPP mode and additional modes which were excited by the grating coupler. It is known that in addition to SPP waves one may excite other waves, such as cylindrical waves [35–38]. Such waves beat with the SPP mode, giving rise to distinct interference patterns, which in our case are helpful in revealing the phase front of the propagating signal.

In this Letter, we describe the design, fabrication, and near-field characterization of a graded-index plasmonic lens. The device was constructed by patterning a layer of PMMA that is positioned on top of a flat Au film. Based on the EMT we found the relation between the duty cycle of the subwavelength grating and the effective index of the SPP mode. Light was coupled into the device via a grating coupler and the propagation of the SPP mode within the device was measured by a near-field microscope. We observed the converging of the plasmonic wavefronts and the focusing of the SPP mode into a distinct waist located about 23.5 μm away from the front end of the lens. Similarly to conventional Gaussian optics, further propagation beyond the focus is accompanied by the expansion of the plasmonic beam and the divergence of the phase front. By combining a simple and binary fabrication procedure, together with the flexibility in controlling the propagation of SPP modes at will open the demonstrated approach is expected to play significant role in future plasmonic applications, such as beam steering, splitting, cloaking, mode matching, and beam shaping.

This research was supported by an AFOSR grant. Boris Desiatov and Ilya Goykhman acknowledge the Eshkol fellowship from the Israeli ministry of science.

References

1. B. Rothenhaulser and W. Knoll, Nature **332**, 615 (1988).
2. K. Giebel, C. Bechinger, S. Herminghaus, M. Riedel, P. Leiderer, U. Weiland, and M. Bastmeyer, Biophys. J. **76**, 509 (1999).
3. L. Berguiga, T. Roland, K. Monier, J. Elezgaray, and F. Argoul, Opt. Express **19**, 6571 (2011).
4. T. Holmgaard, Z. Chen, S. I. Bozhevolnyi, L. Markey, and A. Dereux, Opt. Express **17**, 2968 (2009).
5. R. Charbonneau, N. Lahoud, G. Mattiussi, and P. Berini, Opt. Express **13**, 977 (2005).
6. W. L. Barnes, A. Dereux, and T. W. Ebbesen, Nature **424**, 824 (2003).
7. R. Corn, M. Romagnoli, M. D. Levenson, and M. R. Philpott, Chem. Phys. Lett. **106**, 30 (1984).
8. S. Palomba, Nat. Mater. **11**, 34 (2012).

9. M. E. Stewart, C. R. Anderton, L. B. Thompson, J. Maria, S. K. Gray, J. A. Rogers, R. G. Nuzzo, and M. E. Stewart, Chem. Rev. **108**, 494 (2008).
10. N. Liu, M. Mesch, T. Weiss, M. Hentschel, and H. Giessen, Nano Lett. **10**, 2342 (2010).
11. A. G. Brolo, R. Gordon, B. Leathem, and K. L. Kavanagh, Langmuir **20**, 4813 (2004).
12. W. Srituravanich, N. Fang, C. Sun, Q. Luo, and X. Zhang, Nano Lett. **4**, 1085 (2004).
13. A. Ciatton, C. Rizza, and E. Palange, Phys. Rev. A **83**, 043813 (2011).
14. J. Gu, R. Singh, A. K. Azad, J. Han, A. J. Taylor, J. F. O'Hara, and W. Zhang, Opt. Mater. Express **2**, 31 (2012).
15. P. Ginzburg, A. Nevet, N. Berkovitch, A. Normatov, G. M. Lerman, A. Yanai, U. Levy, and M. Orenstein, Nano Lett. **11**, 220 (2011).
16. A. Nevet, N. Berkovitch, A. Hayat, P. Ginzburg, S. Ginzach, O. Sorias, and M. Orenstein, Nano Lett. **10**, 1848 (2010).
17. A. Yanai and U. levy, J. Opt. Soc. Am. B **27**, 1523 (2010).
18. I. Goykhman, B. Desiatov, J. Khurgin, J. Shappir, and U. Levy, Nano Lett. **11**, 2219 (2011).
19. A. Akbari, R. N. Tait, and P. Berini, Opt. Express **18**, 8505 (2010).
20. M. W. Knight, H. Sobhani, P. Nordlander, and N. J. Halas, Science **332**, 702 (2011).
21. I. Goykhman, B. Desiatov, J. Khurgin, J. Shappir, and U. Levy, Opt. Express **20**, 28594 (2012).
22. Z. Liu, J. M. Steele, W. Srituravanich, Y. Pikus, C. Sun, and X. Zhang, Nano. Lett. **5**, 1726 (2005).
23. G. M. Lerman, A. Yanai, and U. Levy, Nano Lett. **9**, 2139 (2009).
24. T. Zentgraf, Y. Liu, M. H. Mikkelsen, J. Valentine, and X. Zhang, Nat. Nanotechnol. **6**, 151 (2011).
25. J. B. Pendry, D. Schurig, and D. R. Smith, Science **312**, 1780 (2006).
26. U. Levy, M. Abashin, K. Ikeda, A. Krishnamoorthy, J. Cunningham, and Y. Fainman, Phys. Rev. Lett. **98**, 243901 (2007).
27. U. Levy, M. Nezhad, H. C. Kim, C. H. Tsai, L. Pang, and Y. Fainman, J. Opt. Soc. Am. A **22**, 724 (2005).
28. A. V. Kildishev and V. M. Shalaev, Opt. Lett. **33**, 43 (2008).
29. N. Kundtz and D. R. Smith, Nat. Mater. **9**, 129 (2010).
30. V. Nguyen, S. Larouche, N. Landy, J. S. Lee, and D. R. Smith, J. Opt. Soc. Am. A **29**, 2479 (2012).
31. P. A. Huidobro, M. L. Nesterov, L. Martín-Moreno, and F. J. García-Vidal, Nano Lett. **10**, 1985 (2010).
32. Y. Liu, T. Zentgraf, G. Bartal, and X. Zhang, Nano Lett. **10**, 1991 (2010).
33. S. M. Rytov, Sov. Phys. JETP **2**, 466 (1956).
34. A. F. Oskooi, D. Roundy, M. Ibanescu, P. Bermel, J. D. Joannopoulos, and S. G. Johnson, Comput. Phys. Commun. **181**, 687 (2010).
35. W. Dai and C. M. Soukoulis, Phys. Rev. B **80**, 155407 (2009).
36. A. Yu. Nikitin, S. G. Rodrigo, F. J. García-Vidal, and L. Martín-Moreno, New J. Phys. **11**, 123020 (2009).
37. P. Lalanne, J. P. Hugonin, H. T. Liu, and B. Wang, Surf. Sci. Rep. **64**, 453 (2009).
38. F. López-Tejeira, S. G. Rodrigo, L. Martín-Moreno, F. J. García-Vidal, E. Devaux, J. Dintinger, T. W. Ebbesen, J. R. Krenn, I. P. Radko, S. I. Bozhevolnyi, M. U. González, J. C. Weeber, and A. Dereux, New J. Phys. **10**, 033035 (2008).